

# ANALYTICAL PREDICTION AND IN-SITU EXPERIMENTAL CHARACTERIZATION OF ANISOTROPIC FIBROUS MATERIALS

Teresa Bravo<sup>1</sup>, Cedric Maury<sup>2</sup>, Daniel Mazzoni<sup>3</sup>, Muriel Amielh<sup>3</sup>

<sup>1</sup> Spanish National Research Council  
e-mail: teresa.bravo@csic.es

<sup>2</sup> Laboratory of Mechanics and Acoustics (CNRS)  
e-mail: cedric.maury@centrale-marseille.fr

<sup>3</sup> Institute of Research on Non-Equilibrium Phenomena (CNRS)  
email: daniel.mazzoni@centrale-marseille.fr; muriel.amielh@univ-amu.fr

## Resumen

El diseño de materiales acústicos alternativos para problemas de control de ruido ambiental requiere una caracterización experimental que debe realizarse considerando las condiciones in situ para una estimación precisa de sus propiedades absorbentes. En este trabajo estamos interesados en el estudio de materiales fibrosos anisotrópicos como una alternativa a los materiales clásicos que no pueden lograr las reducciones de ruido específicas recomendadas por las organizaciones mundiales de la salud. Sus propiedades, direccionalmente dependientes, proporcionan más grados de libertad para la optimización y adecuación a diferentes problemas. Se predicen utilizando una formulación analítica que tiene en cuenta tanto la anisotropía como la dependencia de la frecuencia del módulo complejo de densidad y compresibilidad y requiere la solución de una ecuación trascendental. La verificación de los resultados se ha realizado de forma experimental con una sonda de presión-velocidad in situ que proporciona los coeficientes de absorción y reflexión en función del diámetro de las fibras. También se han obtenido resultados cubriendo el material fibroso con un panel microperforado.

**Palabras clave:** medida de absorción in situ, materiales fibrosos anisotrópicos, paneles microperforados.

## Abstract

The design of alternative acoustic materials for environmental noise control problems requires an experimental characterization that has to be done considering in-situ conditions for accurate estimation of their absorbing properties. In this work we are interested in the study of anisotropic fibrous materials as an alternative to classical materials that cannot achieve the targeted noise reductions recommended by world health organizations. Their properties, directionally dependent, provide more degrees of freedom for optimization and adequacy to different problems. They are predicted using an analytical formulation that accounts for both anisotropy and frequency dependence of the complex density and compressibility module. It requires the solution of a transcendental equation. Verification of the results has been carried out experimentally with an in-situ pressure-velocity probe that provides the absorption and reflection coefficients as a function of the fibers diameter. Results have also been obtained when shielding the fibrous material by a micro-perforated panel.

**Keywords:** in-situ measurement absorption, anisotropic fibrous materials, micro-perforated panels.

**PACS n°.** 43.20.Rz, 43.50.-x

## 1 Introduction

One of the major contributors to noise pollution in urban environments is the transportation system [1]. Low-frequency broadband noise control constitutes a predominant contribution in the aeronautic and automotive transports [2]. Many acoustic devices for the reduction of fan and jet noise are constituted of liners made up of a honeycomb core bonded to a perforated sheet in contact with the flow that acts as a resistive skin. They provide significant noise attenuation at high frequencies, due to the thickness of the embarked porous material that spans several wavelengths of the incident sound wave, but they also add additional weight and may obstruct fast routine maintenance inspection. Several active flow control technologies have also been studied showing promising results, but still at an early stage [3, 4]. Taking aviation safety and energy consumption into consideration, active flow control methods are mainly applied to downscaled model of airframe components and still have a moderate technology readiness level.

As an alternative to classical materials, layouts of panels with micro-slits or micro-perforations have been considered. These treatments are resonance absorbers composed of Micro-Perforated Panels (MPPs) with sub-millimetric holes backed by an air cavity [5, 6]. They are tuneable control devices with adjustable performance achieved by a proper selection of their physical constitutive parameters. Despite these advantages, MPP-based solutions for real problems are still moderate. The work done until now is mainly intended for room acoustic applications. Knowledge about their acoustic behaviour is still ongoing research for most of the noise problems addressed by the transportation industry. In particular, studies about the finite-size effects of the MPP partitions, their vibrating response [7] as well as their absorption and transmission properties [8, 9] under an acoustic excitation. Recently, the acoustic response of MPPs partition in presence of grazing and/or bias flow [10] has been studied, with relevance to flow noise problems in the automotive industry.

Bio-inspired low-frequency materials have been developed for a long time. In particular, it has been identified that the silent flight of certain species of night bird predators, such as the large owls, can offer insights for the design of multi-layer structures in order to reduce the airframe noise in aeronautic systems [11]. Owls are able to eliminate the self-noise produced during flight by the turbulent pressures in the wing boundary layers and from the legs between 2 and 10 kHz. Such noise reduction relies on the specific plumage of their wings with three main characteristics prone to a silent flight. Apart from the leading edge serrations that prevent boundary layer separation [12] and the trailing edge porous fringes that provide smooth mixing of the upper and lower boundary layers [13], the feathers are coated by a fine, soft downy material evenly distributed on the top of the wings.

From the observed morphology and constitutive parameters of the owl feathers, a number of modelling studies aimed at developing a mimetic surface to demonstrate the reduction of noise caused by flow over the surface. Experimental studies have been presented by Clark *et al.* [14] on surfaces which mimic the morphology and assumed noise reduction properties of owl feathers, with particular attention to the velvety coating on its top surface. They tested several bio-inspired treatments in an anechoic wall-jet facility and analysed the effects on the surface pressure spectra as well as on the far-field sound levels of various rough surfaces, eventually shrouded by a canopy. All canopies had a strong beneficial influence on the surface pressure spectra in the mid-frequency range with up to 30 dB attenuation of the roughness noise at 1500 Hz and for external flow speed of  $20 \text{ m}\cdot\text{s}^{-1}$  with the thinnest filament canopy. Through physical scaling, the authors pointed out that the canopy acted as a spatial filter, responsible of the exponential attenuation of the surface pressures linked to the turbulent eddy scales smaller than the canopy height.

These studies also analysed external effects by studying how the canopy suspended above a rough surface interacts with the flow and reduces the pressure fluctuations in a manner similar to the effect of wind over and through vegetation canopy. The work presented here studies the internal attenuation effects underneath and within the canopy. We deal with the attenuation effects inside a given absorbing partition beneath a uniform flow in order to reproduce the aero-acoustic properties of the velvety down wing surface. In this work we assume that a description appropriate to bio-inspired surface may be the use of fibrous anisotropic materials as they seem well-suited to describe the intricate structure of the owl wing feathers. These materials with a specified solid frame constitute a particular category of a more general class of fluid-solid mixtures, ranging from porous rocks, fibrous and granular solids, foam materials to emulsions and suspensions. The capillary pore approach was first used by Rayleigh [15]. Many later fiber theories were, essentially, generalizations of this approach and introduced phenomenological parameters to allow for deviations from the simple capillary pore structure. The multiple scattering approach [16] is a fruitful model of fibers suspension in the air that incorporates wave motion between and within the fibers which can be randomly distributed and of different radii. It is built upon a cylindrical harmonic decomposition of the incident, scattered dilatational, thermal and viscous waves in the fluid phase, and induced dilatational, thermal and shear waves in the solid phase of the fibers. Although this model is a faithful description of the real problem, it does not account for propagation through anisotropic materials made up of inclined fibers in contact with an external flow.

The starting point of the work presented here is the model of Nayfeh and Sun [17], that describes the axial attenuation of waves propagating in a two-dimensional duct carrying a uniform mean flow and treated by a bulk-reacting liner consisting of an anisotropic porous material backed by a cellular honeycomb core. This model is generalized in the present study by accounting for a fully anisotropic complex compressibility and air flow resistivity. It is used to evaluate numerically and experimentally the absorption properties of rigidly-backed fibrous anisotropic partitions, eventually shielded by a MPP. A theoretical approach that predicts the normal incidence absorption through these treatments will be assessed in Section 2, that generalizes Nayfeh and Sun model to account for anisotropic bulk modulus as well as viscous and thermal diffusion effects. The model will be validated in Section 3 against a set of published results and in laboratory conditions (Section 4) with an *in-situ* impedance probe for different configurations of materials combined with MPPs. The main conclusions and directions for future work will be summarized in the last section.

## 2 Analytical formulation

### 2.1 Theoretical analysis

The configuration to be studied is outlined in Figure 1.

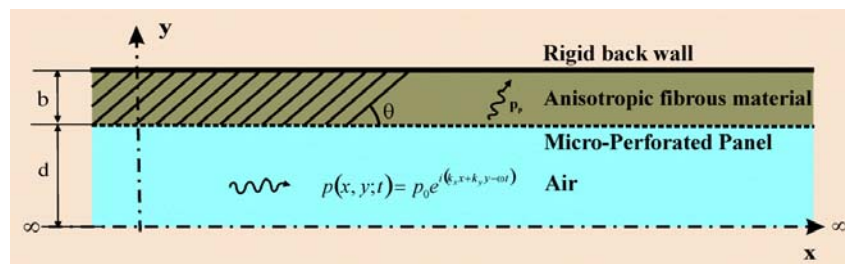


Figure 1 –Physical set-up

It consists of a uniform liner of infinite extent along the  $x$ -axis composed of a thin flexible MPP located at  $y = d$  and separated from a rigid back wall by a layer of anisotropic fibrous material with thickness  $b$ . Acoustic waves ( $e^{-i\omega t}$ ) propagate both in the porous and in the fluid domains. In the following sub-sections, we outline the main equations that predict the absorption properties of several models of anisotropic partitions. We start by a classical model of fibrous material with anisotropic resistivity that accounts for viscous losses along and normal to the fibers. It is subsequently generalized to the case of a fully anisotropic fibrous material with complex effective densities and bulk moduli along and normal to the fiber axis, that respectively account for relaxation effects associated to viscous and thermal diffusion. Finally, we model a rigidly-backed partition composed of a rigid MPP backed by a layer of anisotropic materials

### 2.1.1 Weakly anisotropic model for fibrous materials

The purpose of the formulation is to find analytical expression for the axial attenuation (dB/m) and the normal absorption coefficient  $\alpha$  induced by a rigidly-backed anisotropic fibrous material of thickness  $b$  in contact with a fluid flowing uniformly in the half-space  $y < d$ , as shown in Figure 1. The fibers are inclined at an angle  $\theta$  with respect to the material surface. The pressure and the axial and normal velocities are denoted respectively  $\tilde{p}$ ,  $\tilde{v}_x$  and  $\tilde{v}_y$  in the fluid domain and  $\tilde{p}_p$ ,  $\tilde{v}_{px}$  and  $\tilde{v}_{py}$  in the porous domain, with the generic wave form  $\tilde{g}(x, y; t) = g(y)e^{i(k_x x - \omega t)}$ . Eliminating the density fluctuations  $\tilde{\rho}$ ,  $\tilde{v}_x$  and  $\tilde{v}_y$  between the Euler equation, the mass conservation and the thermodynamic law,  $\tilde{p} = \tilde{\rho}c_0^2$ , leads to the convected Helmholtz-equation satisfied by the pressure in the fluid domain

$$p'' + \left[ (Mk_x - k_0)^2 - k_x^2 \right] p = 0 \quad (1)$$

with  $p'' = d^2 p / dy^2$ ,  $M = U_\infty / c_0$  the flow Mach number with axial velocity  $U_\infty$  and  $c_0$  the sound speed.  $k_0 = \omega / c_0$  and  $k_y$  are the acoustic and axial wavenumbers in the fluid domain. As for the anisotropic fibrous material, the conservation of momentum is expressed in matrix form in terms of the material properties along,  $\tau$ , and normal,  $n$ , to the fiber directions, as follows

$$\frac{\rho_0}{\Omega} \mathbf{S}_\theta \begin{bmatrix} \frac{\partial \tilde{v}_{px}}{\partial t} \\ \frac{\partial \tilde{v}_{py}}{\partial t} \end{bmatrix} + \begin{bmatrix} \frac{\partial \tilde{p}_p}{\partial x} \\ \frac{\partial \tilde{p}_p}{\partial y} \end{bmatrix} + \mathbf{\Sigma}_\theta \begin{bmatrix} \tilde{v}_{px} \\ \tilde{v}_{py} \end{bmatrix} = \begin{bmatrix} 0 \\ 0 \end{bmatrix}. \quad (2)$$

In this expression,  $\mathbf{S}_\theta = \begin{bmatrix} s_{\tau\tau} & s_m \\ s_{n\tau} & s_{nn} \end{bmatrix}$  and  $\mathbf{\Sigma}_\theta = \begin{bmatrix} \sigma_{\tau\tau} & \sigma_m \\ \sigma_{n\tau} & \sigma_{nn} \end{bmatrix}$  are the structure factor and flow resistivity matrices, the elements of which have the form  $s_{\tau\tau} = s_\tau \cos^2 \theta + s_n \sin^2 \theta$ ,  $s_{nn} = s_\tau \sin^2 \theta + s_n \cos^2 \theta$ ,  $s_m = s_{n\tau} = (s_\tau - s_n) \sin 2\theta / 2$ , with the same dependence for the elements of the  $\mathbf{\Sigma}_\theta$  matrix.  $\Omega$  is the porosity defined as the fraction of air volume with respect to the total volume of material and  $s_{\tau(n)}$  are the structure factors along (resp. normal) to the fiber axis. In the same way,  $\sigma_{\tau(n)}$  are the flow resistivities along (resp. normal to) the fibers directions and that account for frictional viscous dissipation effects along and across the fluid-fiber interface.

The equation of mass conservation in the fibrous material can be written as

$$\Omega \frac{\partial \tilde{p}_p}{\partial t} + \mathbf{K}_p \nabla \cdot \tilde{\mathbf{v}}_p = 0, \quad (3)$$

assuming an isotropic lossless bulk modulus given by  $\mathbf{K}_p = \rho_0 c_0^2$ . Operating from Eqs. (1-2) to eliminate  $v_{px}$ ,  $v_{py}$  and  $p'_p$ , we obtain an equation of propagation for the pressure amplitude in the fibrous material in the form

$$p_p''(y) + F_1 p_p'(y) + F_2 p_p(y) = 0, \quad (4)$$

with  $F_1 = -\frac{ik_{px}}{g_{\tau\tau}}(g_m + g_{n\tau})$  and  $F_2 = \frac{i\omega\Omega \det(\mathbf{g})}{\mathbf{K}_p g_{\tau\tau}} - \frac{k_{px}^2 g_{nn}}{g_{\tau\tau}}$  and  $\det(\mathbf{g}) = \begin{vmatrix} g_{\tau\tau} & g_m \\ g_{n\tau} & g_{nn} \end{vmatrix}$ , where we have

used the following notation,  $g_{\tau\tau(nm)} = \sigma_{\tau\tau(nm)} - i\omega\rho_0\Omega^{-1}s_{\tau\tau(nm)}$  and  $g_m = g_{n\tau} = \sigma_m - i\omega\rho_0\Omega^{-1}s_m$ . We can now obtain an expression for the input admittance  $\beta = \rho_0 c_0 \frac{\tilde{v}_{py}(x, d; t)}{\tilde{p}_p(x, d; t)}$  at the interface  $y = d^\mp$  in

terms of either the fluid flow or the material parameters. Applying continuity of the pressure and normal particle displacement at  $y = d^-$  on the fluid side, the input admittance can be expressed in terms of the fluid parameters as

$$\beta = \frac{\omega k_y c_0}{(\omega - U_\infty k_x)^2} = \frac{k_0 k_y}{(k_0 - M k_x)^2}, \quad (5)$$

with  $k_y^2 = (M k_x - k_0)^2 - k_x^2$  and  $\text{Im}(k_y) > 0$ . We can now obtain an expression for this quantity at  $y = d^+$  towards the fibrous material. We assume an expression for the pressure of the form  $\tilde{p}_p(x, d; t) = (a_p e^{ik_{py1}d} + b_p e^{ik_{py2}d}) e^{i(k_x x - \omega t)}$  where  $k_{py1}$  and  $k_{py2}$  are the transverse wavenumbers of the forward and backward waves travelling in the material. Back substituting  $\tilde{p}_p$  into Eq. (4), we obtain a second order polynomial equation, with well-known solutions given by  $2k_{py1,2} = iF_1 \pm \kappa_p$ , with

$$\kappa_p \equiv k_{py1} - k_{py2} = \frac{2\sqrt{\det(\mathbf{g})}}{g_{\tau\tau}} \sqrt{\frac{i\omega\Omega}{\mathbf{K}_b} g_{\tau\tau} - k_x^2}, \quad (6)$$

the phase propagation constant and  $F_1$  the attenuation factor in the transverse  $y$ -direction. An expression for the velocity  $\tilde{v}_{py}$  in the fibrous material can also be obtained when imposing the rigid back wall condition,  $\tilde{v}_{py}(x, b + d; t) = 0$ . Evaluating the ratio between velocity and pressure at  $y = d^+$ , one obtains the following expression for the input admittance of the fibrous material

$$\beta = -\rho_0 c_0 \frac{g_{\tau\tau} \kappa_p}{2 \det(\mathbf{g})} \tan\left(\frac{\kappa_p b}{2}\right). \quad (7)$$

Equating Eqs. (5) and (7) leads to the following eigenvalue problem,

$$\beta = -\frac{\rho_0 c_0 g_{\tau\tau} \kappa_b}{2 \det(\mathbf{g})} \tan\left(\frac{\kappa_b}{2} d\right) = \frac{k_0 k_y}{(k_0 - M k_x)^2}. \quad (8)$$

Eq. (8) have to be solved for each frequency in the complex  $k_x$ -space restrained to  $\text{Im}(k_x) > 0$  in order to avoid exponential growth of the solution when  $x > 0$ . Once the solution is identified, denoting  $z = \beta^{-1}$ , we proceed to calculate the normal absorption coefficient,

$$\alpha = 1 - \left| \frac{z-1}{z+1} \right|^2. \quad (9)$$

### 2.1.2 Fully anisotropic model for fibrous materials

In Eq. (3), the assumption of an isotropic effective velocity, equal to the speed of sound in all directions of the anisotropic material, is rather restrictive and is overcome in this section. A generalized mass conservation equation should include an anisotropic bulk modulus with values  $K_\tau$  along the fiber axis and  $K_n$  normal to the plane of the fibers. Eq. (3) of mass conservation is then updated as

$$\Omega \frac{\partial \tilde{p}_p}{\partial t} + \text{Tr}[\mathbf{K} \nabla \tilde{\mathbf{v}}_p] = 0, \quad (10)$$

where  $\mathbf{K} = \begin{bmatrix} K_{\tau\tau} & K_m \\ K_{n\tau} & K_{nn} \end{bmatrix}$  is the bulk modulus matrix whose elements follow the same construction rule as those of the structure factor and flow resistivity matrices (Eq. 2). The complex bulk moduli  $K_\tau$  and  $K_n$  can be defined as a function of the flow resistivities,  $\sigma_\tau$  and  $\sigma_n$ , along and normal to the fiber axis, as follows [18]

$$K_{\tau,n} = \rho_0 c_0^2 \left\{ 1 + \frac{(\gamma-1)}{\sqrt{1 - \frac{4i\omega\rho_0 N_p}{\sigma_{\tau,n}}}} \right\}^{-1}, \quad (11)$$

where  $\gamma = C_p/C_v$  is the ratio of the heat capacities at constant pressure and volume, and  $N_p = C_p\eta/\kappa_T$  the Prandtl number with  $\kappa_T$  the thermal conductivity. We also derive a generalized form of the momentum conservation equation with the following complex effective mass densities

$$\rho_{0\tau,n} = \rho_0 \left\{ 1 - \frac{1}{\sqrt{1 - \frac{2i\omega\rho_0}{\sigma_{\tau,n}}}} \right\}^{-1}. \quad (12)$$

The corresponding notations used in this section have to be updated as  $g_{\tau\tau(nm)} = \sigma_{\tau\tau(nm)} - i\omega\rho_{p,\tau\tau(nm)}\Omega^{-1}$ ,  $g_m = g_{n\tau} = \sigma_m - i\omega\rho_{p,m}\Omega^{-1}$  with the following definitions  $\rho_{p\tau\tau} = \rho_{0\tau}s_\tau \cos^2 \theta + \rho_{0n}s_n \sin^2 \theta$ ,  $\rho_{pnm} = \rho_{0\tau}s_\tau \sin^2 \theta + \rho_{0n}s_n \cos^2 \theta$  and  $\rho_{p_m} = \rho_{p_{n\tau}} = (\rho_{0\tau}s_\tau - \rho_{0n}s_n) \sin \theta \cos \theta$ . The coefficients of the wave propagation equation (4) now take the form

$$F_1 = -\frac{ik_x(K_{\tau\tau}g_m + K_{nn}g_{n\tau} - K_m g_{nn} - K_{n\tau}g_{\tau\tau})}{K_{nn}g_{\tau\tau} - K_{n\tau}g_m} = -ik_x F'_1, \quad (13)$$

$$F_2 = -\frac{i\omega\Omega \det(\mathbf{g}) - k_x^2(K_{\tau\tau}g_{nn} - K_m g_{n\tau})}{K_{nn}g_{\tau\tau} - K_{n\tau}g_m}. \quad (14)$$

With these coefficients, Eq. (4) is generalized to the case of a fully anisotropic fibrous material with complex bulk moduli and effective densities associated to thermal and viscous diffusion effects along and across the fibers. The specific input impedance of the fibrous material is then expressed as

$$z = \beta^{-1} = \frac{[-ik_x(g_{n\tau} + \kappa_a) + g_{\tau\tau}\kappa_p \cot(\kappa_p b/2)] \det(\mathbf{g})}{2Z_0(k_x^2 g_{n\tau} \kappa_a - F_2 g_{\tau\tau}^2)}, \quad (15)$$

with  $\kappa_a = g_{nr} - g_{\tau\tau} F_1'$  and  $F_1'$  calculated from Eq. (13).  $\alpha$  is then deduced from Eq. (9) evaluated at the zeros of the transcendental equation,  $\beta = k_0 k_y (k_0 - M k_x)^{-2}$ , that replaces Eq. (8).

### 2.1.3 Model for anisotropic materials shielded by a rigid MPP

The overall transfer impedance,  $Z_{\text{MPP}}/\sigma$ , for a rigid MPP with circular holes of diameter  $d_h$  and thickness  $t_h$  is given by the expression [5, 6]

$$\frac{Z_{\text{MPP}}}{\sigma} = \frac{32\eta t_h}{\sigma d_h^2} \left[ \sqrt{1 + \frac{k_h^2}{32}} + \frac{\sqrt{2}}{32} k_h \frac{d_h}{t_h} \right] - i\rho_0 \omega \frac{t_h}{\sigma} \left[ 1 + \left( 9 + \frac{k_h^2}{2} \right)^{-1/2} + \frac{8}{3\pi} \frac{d_h}{t_h} \right], \quad (16)$$

with  $\sigma$  the perforation ratio,  $\eta$  the dynamic viscosity of the air, and  $k_h = (d_h/2)/r_{\text{visc.}}(\omega)$ , the perforate constant, e.g. the ratio of the hole radius to the viscous boundary layer thickness,  $r_{\text{visc.}}(\omega) = \sqrt{\eta/\rho_0\omega}$ , with  $\rho_0$  the air density. Eq. (16) is valid provided that  $b_h < \lambda/4$ , with  $b_h$  the holes pitch,  $\lambda$  the acoustic wavelength and  $b_h \gg d_h$  to neglect holes interaction effects.

In this section, we develop a model to study how the absorption of rigidly-backed thin MPPs is modified when lined with anisotropic fibrous materials. We still need to solve an eigenvalue equation in the  $k_x$ -complex plane that equates the specific input admittance  $\beta$  of the fibrous material at  $y = d^+$  and the specific admittance on the MPP inner side,  $1/z_d^+$ .  $z_d^+$  is related to the specific input impedance at the MPP outer side,  $y = d^-$ , as follows

$$z_d^+ = z_d^- - \frac{(p - p_p)}{Z_0 v_y} = z_d^- - \frac{Z_{\text{MPP}}}{Z_0 \sigma}, \quad (17)$$

where the assumption of a rigid MPP has been made for the last term in Eq. (17). This specific impedance on the flow side can be expressed according to Eq. (5) as  $1/z_d^- = k_0 k_y / (k_0 - M k_x)^2$ .

Considering that  $\beta = 1/z_d^+$ , we obtain from Eq. (17) the eigen-equation

$$\beta = \frac{k_0 k_y}{(k_0 - M k_x)^2 - \frac{k_0 k_y}{Z_0} \frac{Z_{\text{MPP}}}{\sigma}}, \quad (18)$$

with  $\beta$  related to either Eq. (7) or (15). The absorption coefficient is then calculated from Eq. (9) as

$$z = z_d^- = \frac{Z_{\text{MPP}}}{Z_0 \sigma} + \frac{1}{\beta}. \quad (19)$$

## 3 Comparison with previous results

To assess the analytical models presented in the previous section, it is necessary to solve the eigenvalue problems associated to the transcendental Equations (8, 15, 18). This can be viewed as an optimization problem that has to be solved for the unknown complex variable  $k_x$  for each frequency of analysis. Due to the computational cost of this combinatorial problem, an exhaustive search method would be too lengthy to be carried out. In this work we have selected the simulated annealing method [19] to find the global optimal solution. This method is well-suited for large-scale non-convex optimization problems in which a global solution of minimum

"energy" coexist with many local minima. Also, it has a relatively simple implementation. The algorithm is based on an analogy with the Boltzmann law of thermodynamics that governs the way liquids freeze and crystallize, or the metals cool and anneal, slow cooling reducing the probability for the solution to be trapped in a local minimum. The optimization procedure involves the definition of a space of configurations to be searched that includes the range of variation of all the physical parameters that are selected, here  $\text{Re}(k_x)$  and  $\text{Im}(k_x)$ , and the definition of an objective function that evaluates the performance of the algorithm for all the possible physical configurations. Here the objective function is the absolute value of the difference between the left-hand side and the right-hand side of Equations (8, 16, 19). The optimal results have been selected for the least attenuated mode in the complex  $k_x$ -space, e.g. corresponding to the smallest positive values of  $\text{Im}(k_x)$ . Once the solution is identified, we can proceed with Equations (8, 15, 19) to calculate the specific input admittance of the absorbent and with Equation (9) for its normal absorption coefficient. These analytical models are compared against a set of experimental measurements obtained from either previously published results or from *in-situ* measurements.

A first validation of the models outlined in section 2 considers the results published by Attenborough [20] using free-surface anisotropic materials with parallel horizontal fibers of small diameters. He measured the normal incidence absorption coefficient of different types of fiberglass materials for comparison with the multiple scattering theory (MST) developed in [20]. For each frequency the microphone was located at the pressure nodes and antinodes and the absorption coefficient was deduced from the standing wave ratio. Figure 2 presents the results obtained for a RockSil fiberglass material of thickness 2.54 cm, bulk density  $\rho_b = 28.8 \text{ kg.m}^{-3}$  and calculated porosity  $\Omega = 98.7\%$ , defined as  $\Omega = 1 - V_f$ ,  $V_f = \rho_b / \rho_g$  being the volume density of fibers and  $\rho_g = 2300 \text{ kg.m}^{-3}$  the glass density. The measurements are reproduced as circles on the blue curve for comparison with the different prediction models. In particular, we have included the MST (blue) and the two aforementioned models, weakly (dashed red) and fully anisotropic (red). We also plotted the revised version by Miki [21] of the Delany and Bazley model [22], denoted MDB model. It is valid for locally-reacting porous materials with a porosity close to one and extends the validity of the DB model,  $0.01 < \rho_0 f / \sigma_n < 1$ , at low frequencies.

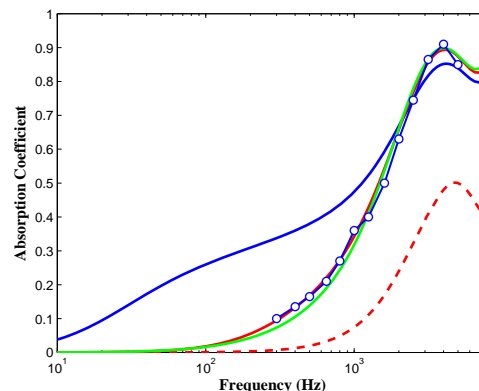


Figure 2 – Normal incidence absorption coefficient for a fiberglass material with bulk density  $28.8 \text{ kg.m}^{-3}$ , and thickness 2.54 cm : comparison between impedance tube measurements (blue with circles, from Fig.5c in [20]) and predictions from the Miki-Delany-Bazley model (solid green), MST (solid blue), weakly (dashed red) and fully (solid red) anisotropic models.

As it can be appreciated, the agreement between the fully anisotropic model and the measurements is remarkable over a broad frequency range between 300 Hz and 5 kHz, and up to 8 kHz when compared to the MDB model. It can also be shown that the weakly anisotropic model significantly underestimates the normal absorption coefficient over the whole frequency range. In either model, a locally reacting material ( $\sigma_{\tau\tau} \gg \sigma_{nn}$ ) has been assumed with parallel identical cylindrical fibers of radius  $a_f = 7 \mu\text{m}$  placed randomly in a horizontal plane ( $\theta = 0^\circ$ ).

This configuration leads to a normal resistivity  $\sigma_{nn} = \sigma_n = 8974 \text{ N.s.m}^{-4}$  if one uses Tarnow's derivation of resistivity to flow perpendicular to a random lattice of parallel fibers [18], e.g.  $\sigma_n = 4\pi\eta N_f / [-0.64\ln(V_f) - 0.737 + V_f]$  with  $N_f = V_f / (\pi a_f^2)$  the concentration of fibers per square meters in a plane perpendicular to the fibers axis. Although not shown, simulations assuming a non-locally reacting material ( $\sigma_{\tau\tau} = \sigma_{nn}/2$ ) underestimate the maximum absorption values, especially at the first quarter wavelength resonance (3376 Hz). Indeed, the models provide an axial wavenumber solution on the least attenuated mode. The agreement is fair when comparing the MST with the measurements above 2 kHz. But below 1 kHz, the correlation with the MST is gradually lost as frequency decreases. The MST based on non contact freely suspended fibers clearly overestimates the absorption as it does not account for the air and fibers that tend to move together in this frequency range, and so reduce the amount of dissipation. Note that a good agreement is maintained between the MDB and the fully anisotropic models at very low frequencies.

## 4 Experimental verification

A series of measurements has been carried out for *in-situ* free-field characterization of the surface impedance and normal absorption coefficient for a number of anisotropic fibrous materials. The measurements have been performed in the LMA semi-anechoic room above the room cut-off frequency of 70 Hz. We have used an absorption measurement device based on a collocated  $p$ - $v$  probe hand held at 2 cm above a contained  $0.5 \text{ m} \times 0.6 \text{ m}$  sample material. The  $p$ - $v$  [23] probe is able to acquire both pressure and normal particle velocity without the restrictions of the classical methods such as the Kundt tube (small sample size, limited frequency range) and the reverberant chamber method (large sample size, background noise). A photograph of the device used for the measurements is presented in Fig. 3.



Figure 3 – Photograph of the  $p$ - $v$  probe used in laboratory conditions for the determination of the absorption coefficient *in-situ*

The  $p$ - $v$  probe is maintained at a constant distance (0.26 m) and decoupled from a piston-on-a-sphere sound source for both free-field impedance calibration prior to the measurements and during measurements of the field impedance over the sample. A mirror source model allowed to deduce the material input impedance, and so the absorption coefficient, from the measured field impedance.

Several tests at the same position above the material showed a good reproducibility of the absorption curves, provided that a moving average technique was applied in the frequency domain to remove the effect of the reflections from the rigid floor surrounding the container, although a short probe-sample stand-off distance already limits the amplitude of the reflections at the probe position. Figure 4 compares the normal absorption curves measured by the  $p$ - $v$  probe over a thin MPP shielding a layer of fiberglass material against predictions from the MDB, weakly anisotropic and fully anisotropic models. As in Fig. 2, the anisotropic models assumed a locally-reacting fibrous material.

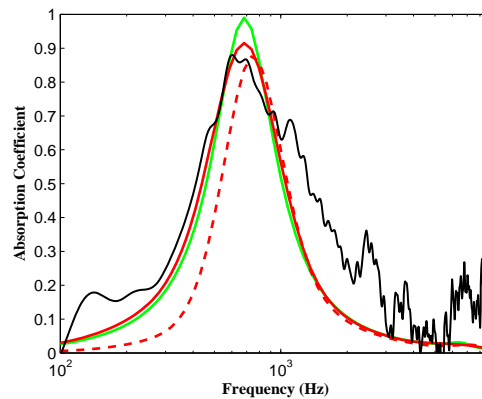


Figure 4 – Normal incidence absorption coefficient for a partition composed of a 1 mm thick aluminium MPP with 0.5 mm holes diameter and 0.87% perforation ratio shielding a layer of fiberglass material with bulk density  $28.8 \text{ kg}\cdot\text{m}^{-3}$  and thickness 2 cm : comparison between  $p$ - $v$  probe measurements (black) and predictions from the MDB (solid green), weakly (dashed red) and fully (solid red) anisotropic models.

It can be seen that the frequency of maximum absorption observed at the Helmholtz-type resonance (680 Hz) is well-predicted by the MDB and the fully anisotropic model, but somewhat overestimated by the weakly anisotropic model. Also, the latter model tends to minimize the absorption bandwidth as it does not fully account for all the dissipation processes within the material. The MDB model clearly overestimates the absorption peak value, but provides a predictive half-bandwidth similar to the fully anisotropic model. The latter model clearly shows the best agreement with the experiment as for the absorption curve, even though the MPP is assumed to be rigid. This may explain why it overestimates the absorption peak value. Considering an elastic MPP with a reduced air-frame relative velocity should improve the correlation at and around the Helmholtz resonance.

We note that all the models assume infinite partitions and so, underpredict the measured absorption values by at least 10% above 1 kHz. Plots of the measured surface impedance showed that these absorption peaks are due to MPP structural resonances that appear as circles folded around the simulated impedance curve associated to an infinite MPP. Therefore, these models cannot capture the beneficial influence of these modes.

## 5 Conclusions

Inspired by the coupling absorption mechanisms of a typical silent flying bird above 1.6 kHz, we suggest that this passive mechanism may be exploited to underlie the design of aircraft fuselage surface able to attenuate the turbulent sound at the source using a combination of micro-slitted and/or micro-perforated flexible membranes shielding layers of porous and fibrous materials in order to achieve such broadband absorption performance. A generalized model has been developed that accounts for full anisotropy of the complex bulk moduli and of the effective density along and across the fibers while including coupling with a uniform external flow. It has been assessed against a set of published impedance tube measurements that evaluate the normal incidence absorption coefficient of fiberglass samples, and also against a set of *in-situ* free-field measurements performed with a *p-v* probe, in particular above a MPP enclosing a layer of rigidly-backed fiberglass material.

The validity of the fully anisotropic model has been ascertained on locally-reacting small-diameter fibers, but also when the fibrous material was shielded by a thin MPP. It can thus be used with confidence to determine which key parameters amongst the parallel and normal flow resistivity, the parallel and normal structure factor, the fibers inclination angle influences the most the normal absorption coefficient, and when shielded by a MPP, the air-frame relative velocity in the MPP holes. The fully anisotropic model should also be further developed to account for an elastic MPP or membrane since we are interested in a model in which the fibrous material should be covered by a compliant thin elastic surface.

## Acknowledgements

This work is part of the project TED2021-130103B-I00, funded by MCIN/AEI/10.13039/501100011033 and the European Union “Next Generation EU”/PRTR, and project PID2022-139414OB-I00 funded by MCIN/AEI/10.13039/501100011033/ and by "ERDF A way of making Europe". It has also received support from the French government under the France 2030 investment plan, as part of the Initiative d'Excellence d'Aix-Marseille Université - A\*MIDEX (AMX-22-RE-AB-157). The authors are grateful to E. Bertrand for their technical and experimental support during the wind-tunnel testing at IRPHE Laboratory.

## References

- [1] WHO, Environmental Noise (2021), <https://www.euro.who.int/en/health-topics/environment-and-health/noise/environmental-noise-guidelines-for-the-european-region>.
- [2] Leylekian, L., Lebrun, M. & Lempereur, P. (2017). An overview of aircraft noise reduction technologies, *Aerospace Lab Journal*, Vol. 7, AL07-01.
- [3] Chan, S., Zhang X. & Gabriel, S. (2007). The attenuation of cavity tones using plasma actuators, *AIAA Journal*, Vol. 45, 1525–1538.
- [4] Oerlemans, S. & Bruin, A. (2009). Reduction of landing gear noise using an air curtain, *Proceedings of the 15th AIAA/CEAS Aeroacoustics Conference*, AIAA, Miami, Florida, 11-13 Mai, pp. 2009-3156.
- [5] Maa, D. Y. (1998). Potential of microperforated panel absorbers, *Journal of the Acoustical Society of America*, Vol. 104, 2861–2866.

- [6] Maa, D. Y. (1997). Microperforated-panel wideband absorbers, *Noise Control Engineering Journal*, Vol. 29, 77–84.
- [7] Bravo, T., Maury, C. & Pinhede, C. (2012). Sound absorption and transmission through flexible micro-perforated panels backed by an air layer and a thin plate, *Journal of the Acoustical Society of America*, Vol. 131, 3853–3863.
- [8] Bravo, T., Maury, C. & Pinhede, C. (2012). Vibroacoustic properties of thin micro-perforated panel absorbers, *Journal of the Acoustical Society of America*, Vol. 132, 789–798.
- [9] Bravo, T., Maury, C. & Pinhede, C. (2014). Optimising the absorption and transmission properties of aircraft microperforated panels, *Applied Acoustics* Vol. 79, 47–57.
- [10] Bravo, T., Maury, C. & Pinhede, C. (2017). Absorption and transmission of boundary layer noise through flexible multi-layer micro-perforated structures, *Journal of Sound and Vibration* Vol. 395, 201–223.
- [11] Graham, R.R. (1934). The silent flight of owls, *Journal of Royal Aeronautic Society* Vol. 38, 837–843.
- [12] Geyer, T.F, Claus, V.T., Sarradj, T & Markus, P.M. (2016). Silent owl flight: the effect of the leading edge comb on the gliding flight noise. *22nd AIAA/CEAS Aeroacoustics Conference*, Lyon, France, pp. 2016-3017.
- [13] Jaworski, J.W. & Peake, N. (2013). Aerodynamic noise from a poroelastic edge with implications for the silent flight of owls, *Journal of Fluid Mechanics*, Vol. 723, 456–479.
- [14] Clark, I.A., Daly, C., Devenport, W., Alexander, W.N., Peake, N., Jaworski, J.W. & Glegg, S., (2016). Bio-inspired canopies for the reduction of roughness noise, *Journal of Sound and Vibration*, Vol. 385, 33–54.
- [15] Rayleigh, L. (1945). *Theory of Sound*. Dover publications, 2nd edition, New York.
- [16] Attenborough K, Walker LA.(1970). Scattering theory for sound absorption in fibrous media. *Journal of the Acoustical Society of America*, Vol. 49(5), 1331-38.
- [17] Nayfeh AH & Sun J. (1975). Sound attenuation in two-dimensional ducts with anisotropic liners. *Journal of Sound and Vibration*, Vol. 41, 421-32.
- [18] Tarnow V. (2002). Measured anisotropic air flow resistivity and sound attenuation of glass wool. *Journal of the Acoustical Society of America*, Vol. 111, 2735-39.
- [19] Press WP, Teukolsky SA, Vetterling WT, Flannery BP. (2007). *Numerical Recipes. The Art of Scientific Computing*. Cambridge University Press, New York.
- [20] Attenborough K. *Sound dissipation in porous media*, PhD Thesis 1969, Department of Civil Engineering, The University of Leeds, United Kingdom.
- [21] Miki Y. (1990). Acoustical properties of porous materials - Modifications of Delany-Bazley models. *Journal of the Acoustical Society of Japan*, Vol. 11, 19-24.
- [22] Delany M, Bazley E. (1970). Acoustic properties of fibrous absorbent materials. *Applied Acoustics*, Vol. 3, 105-16.
- [23] Tijs E. Study and Development of an In Situ Acoustic Absorption Measurement Method. PhD Thesis 2013, University of Twente, The Netherlands.